


Microfluidic fluorescence-activated cell sorting (μ FACS) chip with integrated piezoelectric actuators for low-cost mammalian cell enrichment

Zhen Cheng^{1,2} · Xudong Wu¹ · Jing Cheng^{1,3} · Peng Liu¹ 

Received: 11 September 2016 / Accepted: 1 January 2017 / Published online: 6 January 2017
© Springer-Verlag Berlin Heidelberg 2017

Abstract A low-cost, microfluidic fluorescence-activated cell sorting (μ FACS) microchip integrated with two piezoelectric lead–zirconate–titanate actuators was demonstrated for automated, high-performance mammalian cell analysis and enrichment. In this PDMS–glass device, cells were hydrodynamically focused into a single file line in the lateral direction by two sheath flows, and then interrogated with a forward scattering and confocal fluorescent detection system. The selected cells were displaced transversely into a collection channel by two piezoelectric actuators that worked in a pull–push relay manner with a minimal switching time of ~ 0.8 ms. High detection throughput (~ 2500 cells/s), high sorting rate (~ 1250 cells/s), and high sorting efficiency ($\sim 98\%$) were successfully achieved on the μ FACS system. Six cell mixture samples containing 22.87% of GFP-expressing HeLa cells were consecutively analyzed and sorted on the chip, revealing a stable sorting efficiency of $97.7 \pm 0.93\%$. In addition, cell mixtures containing 37.65 and 3.36% GFP HeLa cells were effectively enriched up to 83.82 and 78.51%, respectively,

on the microchip, and an enrichment factor of 105 for the low-purity (3.36%) sample was successfully obtained. This fully enclosed, disposable microfluidic chip provides an automated platform for low-cost fluorescence-based cell detection and enrichment, and is attractive to applications where cross-contamination between runs and aerosol hazard are the primary concerns.

Keywords Fluorescence-activated cell sorter (FACS) · Microfluidics · Microfabrication · Cell sorting · Piezoelectric actuation

1 Introduction

Fluorescence-activated cell sorting (FACS) has become an indispensable tool for applications in biomedical researches and disease diagnostics (Jaye et al. 2012; Macey 2007; Preffer and Dombkowski 2009), where a large amount of particles (e.g., cells or beads) need to be probed at a single-particle resolution, or a subpopulation of particles (e.g., hematopoietic stem cells or circulating tumor cells) need to be isolated from complex mixtures for downstream characterizations (Magbanua and Park 2013; Naujok et al. 2010). Commercial FACS systems, such as BD FACSAria™ III (East Rutherford, NJ) and Bio-Rad S3™ cell sorter (Hercules, CA), are already able to perform cell analysis and sorting with multi-parametric detections (6-channel fluorescent signals) at an extraordinary speed (10,000 cells/s) (Ibrahim and van den Engh 2003). While effective, FACS is still plagued with several intrinsic drawbacks: First, the current benchtop FACS is expensive, bulky, and the one that requires dedicated maintenance and well-trained operators. As a result, FACS instruments are usually owned and maintained by central laboratories, and their

Electronic supplementary material The online version of this article (doi:10.1007/s10404-017-1847-1) contains supplementary material, which is available to authorized users.

✉ Peng Liu
pliu@tsinghua.edu.cn

¹ Department of Biomedical Engineering, School of Medicine, Collaborative Innovation Center for Diagnosis and Treatment of Infectious Diseases, Tsinghua University, Beijing 100084, Haidian District, China

² Department of Precision Instrument, School of Mechanical Engineering, Tsinghua University, Beijing 100084, China

³ National Engineering Research Center for Beijing Biochip Technology, Beijing 102206, China

availability to individual researchers who have specific demands is dramatically weakened. Second, most FACS systems employ the electrostatic mechanism for sorting, in which particles need to be packaged into tiny droplets and jetted into air for deflection (Shapiro 2005). The resulted aerosols may become a serious safety concern when pathogenic samples are analyzed (Holmes et al. 2014; Schmid et al. 2007). Third, since all the samples that analyzed by a FACS instrument need go through the same tubing and flow cuvette, cross-contamination between runs could be problematic, especially when single-cell analysis, such as single-cell genome sequencing, is performed (Gawad et al. 2016). Apparently, a new flow sorting technique that can avoid these drawbacks while still providing a comparable performance to current FACS systems is highly desired.

Microfluidic FACS system (μ FACS) has been proved to possess several invaluable advantages for flow-based cell analysis and sorting, including enclosed operation environment within a single microdevice, cross-contamination free by making microdevices disposable, and miniaturized footprints for easy deployment (Franke et al. 2010; Godin et al. 2008; Ho et al. 2005; Kim et al. 2011). Therefore, the last two decades have witnessed a great progress of μ FACS systems that utilized diverse physical mechanisms for cell sorting (Osborne 2011; Wyatt Shields IV et al. 2015; Yu et al. 2014). Fu et al. (1999) demonstrated a completely microfabricated FACS device employing electroosmotic flows for sorting *E. coli* cells at a throughput of 20 cells/s (Fu et al. 1999). Following this pioneer work, thermoreversible liquid polymers were explored to form a switching valve, providing a sorting rate of 5 cells/s with a flow velocity of less than 1 mm/s (Shirasaki et al. 2006; Sugino et al. 2009). In addition, both external check (Fu et al. 2002; Wolff et al. 2003) and solenoid valves (Cao et al. 2013; Wu et al. 2013) were integrated into μ FACS to achieve a throughput of 44 cells/s with a 39% yield for *E. coli* and 30 droplets/s for droplets, respectively. The relatively slow response time of these bulky mechanical valves made the further increase in the sorting throughput extremely hard. Instead of switching flows, optical tweezers directly manipulate cells, providing a noninvasive approach for cell isolation (MacDonald et al. 2003). Due to the cell inhomogeneity in optical properties, though, optical forces can only reach a sorting throughput of 100 cells/s with an 82.5% purity (Perroud et al. 2008; Wang et al. 2005). To further improve the sorting rate, Sciambi et al. successfully coupled the dielectrophoretic force with a novel microfluidic structure, in which the collection and the waste outlets were partially divided, allowing 30,000 droplets/s sorting with a 99% accuracy (Sciambi and Abate 2015). However, this great design was only demonstrated to sort droplets not for cells. Bubble expansion force generated by a

pulsed laser was also employed to reach a high-throughput sorting of 23,000 cells/s with a 90% purity in a microfluidic device, although the 8-ns pulsed laser with a high power may hinder the miniaturization of the setup (Chen et al. 2014, 2013). Recently, several microchip-based sorting systems have already been launched onto the market. For examples, Owl biomedical (Santa Barbara, CA) developed a disposable MEMS (microelectromechanical systems) chip that was magnetically actuated for cell sorting. Cytonome (Boston, MA) provided a microchip-based cell sorting system that combined 24 or more microsorters in parallel to achieve ultrahigh-throughput cell analysis. These achievements proved that microfluidic FACS systems can indeed play significant roles in the field of cell sorting.

Among all the sorting mechanisms reported so far, piezoelectric force was believed to well meet the balance between the performance and the cost (Cho et al. 2010). As early as 1989, piezoelectric disc had already been integrated with capillaries for low-cost cell sorting (Gray et al. 1989). Cho et al. (2010) first integrated a piezoelectric actuator into a microfluidic device for hydrodynamic manipulation of cells, demonstrating an enrichment of target mammalian cells with a purity of <60% at a 1000 cells/s throughput (Chen et al. 2011; Cho et al. 2010). While this work proved that piezoelectric μ FACS holds promise to meet cost, size, and performance goals simultaneously, its performance, including the throughput and the purity, still have room for improvement, and its fluorescence-only detection as well as the wave-guided illumination is insufficient for practical cell analysis. In this study, we demonstrated a low-cost μ FACS microchip featured with two on-chip piezoelectric lead–zirconate–titanate (PZT) actuators for high-throughput cell detection and sorting. Within this PDMS–glass hybrid microdevice, cells were hydrodynamically focused into a single file line, and then interrogated with a forward scattering and a confocal fluorescent detector. The selected cells were deflected laterally into a collection channel using two piezoelectric actuators that worked in a pull–push relay manner with a minimal switching time of ~ 0.8 ms. This relay switch significantly reduced the vibration of the focused stream, leading to a higher sorting rate. We thoroughly optimized the microchip structures and the actuation parameters for flow deflection in order to maximize the cell sorting performance. GFP-expressing HeLa cells diluted in the non-fluorescent cell background were employed to test the throughput and the sorting accuracy of this μ FACS system. Our work verified the feasibility of performing high-performance cell sorting using the piezoelectric actuating mechanism. With the improvements on the actuation manner as well as the detection system, the μ FACS has a great potential to deliver a high-purity and high-throughput cell sorting running on a compact

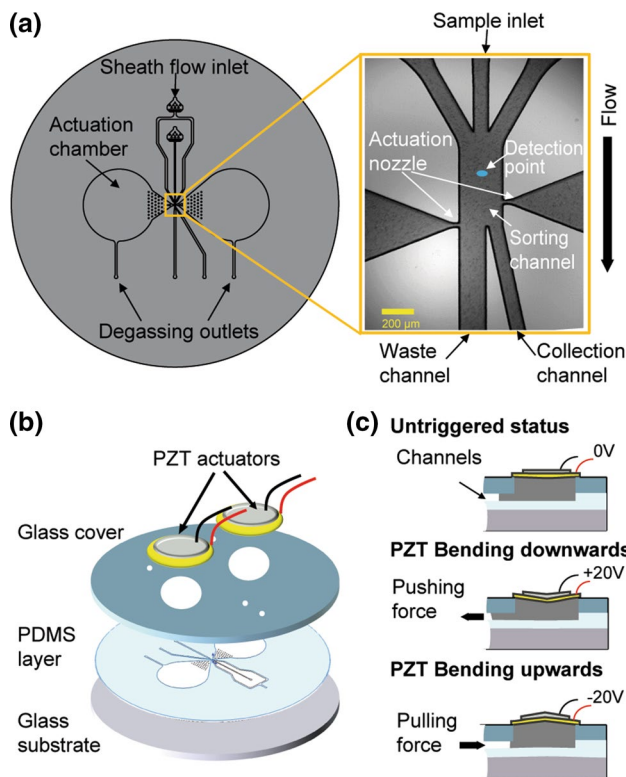


Fig. 1 Schematic of the microfluidic FACS microchip and the piezoelectric actuation mechanism. **a** Structure of the microfluidic chip. The central structure of the microchip is a sorting channel with dimensions of $560\ \mu\text{m}$ in length, $240\ \mu\text{m}$ in width, and $35\ \mu\text{m}$ in height. A cell input channel and two sheath flow channels converge together to form a converging junction at one end of the sorting channel, while a collection and a waste channel are at the other end. The detection point is located on the central line of the sorting channel downstream the converging junction with a distance of $250\ \mu\text{m}$. Two actuation nozzles with tapered structures are designed on both sides of the sorting channel. **b** Exploded view of the microchip structure. The microfabricated PDMS layer with the feature side facing up is sandwiched between two glass wafers. Two PZT actuators are cemented onto the top surface of the microdevice. **c** Illustration of the actuation mechanism. When a $+20\ \text{V}_{p-p}$ signal is sent to the PZT actuator, the PZT bends downwards and squeezes the solution out of the actuation chamber to generate a pushing force. On the contrary, a $-20\ \text{V}_{p-p}$ signal causes the upward bending of the PZT, resulting in a pulling force in the microchannel

instrument with a low cost for a variety of cell enrichment applications in the future.

2 Materials and methods

2.1 Microfluidic chip fabrication

As shown in Fig. 1, the central structure of this μFACS microchip is a sorting channel with dimensions of $560\ \mu\text{m}$ in length, $240\ \mu\text{m}$ in width, and $35\ \mu\text{m}$ in height. A cell input channel and two sheath flow channels, all of which

are $80\ \mu\text{m}$ wide, are converging together to form a converging junction at one end of the sorting channel, while a collection and a waste channel are at the other end. These two outlet channels are designed to be asymmetrically wide in order to let the unwanted cells flow straightly into the waste channel. The detection point is located on the central line of the sorting channel downstream the converging junction with a distance of $250\ \mu\text{m}$. Two actuation nozzles with tapered connecting structures are designed on both sides of the sorting channel, and are 390 and $510\ \mu\text{m}$ away from the converging junction, respectively. In the end of each actuation nozzle is a 25-mm -diameter actuation chamber covered with a piezoelectric actuator from the top. As indicated in Fig. 1a, each actuation chamber also has another output channel for degassing purpose.

The structure of this μFACS microchip, as illustrated in Fig. 1b, consists of three layers (from top to bottom): a glass cover layer with two integrated PZT actuators and drilled via holes, a polydimethylsiloxane (PDMS) microfluidic layer with microstructures on the upper side, and a bare glass substrate for supporting. The PDMS layer was fabricated using the replica molding as reported previously (Duffy et al. 1998). Briefly, the casting mold was photolithographically fabricated on a $4''$ silicon wafer with $35\text{-}\mu\text{m}$ -thick SU-8 photoresists (MicroChem, Westborough, MA). Next, PDMS (10:1, PDMS: curing agent, Sylgard[®] 184, Dow Corning, Midland, MI) was cast onto the mold, followed by the curing process at $80\ ^\circ\text{C}$ for 1 h. The cured PDMS was then peeled off from the mold and trimmed to the suitable size. To enclose the PDMS structures and to further enhance the rigidity of the chip, the PDMS layer with the feature side facing up was sandwiched between two $4''$ glass wafers (BF33, Gous Optical, Shanghai, China), the top of which was drilled with via holes and the actuation holes using a numerical drilling machine (54103A, Sherline, Vista, CA) and the bottom of which was left blank. The permanent bonding between this wafer stack was achieved using oxygen plasma (Femto, Diener Electronic, Nagold, Germany). The PZT actuators (2.6 kHz PUI transducers, Mouser Electronics, Mansfield, TX) were cemented onto the top glass layer with a UV glue (Loctite 3491, Henkel, Duesseldorf, Germany). Steel pipe connectors were also glued to each via hole for connecting with PTFE tubing (The Lee Company, Westbrook, CT). After the fabrication process, the entire μFACS microchip was filled with DI water and vacuumed in an oven for an hour to expel air out completely. Once no bubbles were left in the chip, especially in the actuation chambers, the degassing outlets were completely sealed with two pieces of adhesive tape (MSB 1001, Bio-Rad, Hercules, CA), and all the other inlets and outlets were plugged. Until use, the primed chip was stored in $4\ ^\circ\text{C}$ to ensure no bubble generated during the storage period.

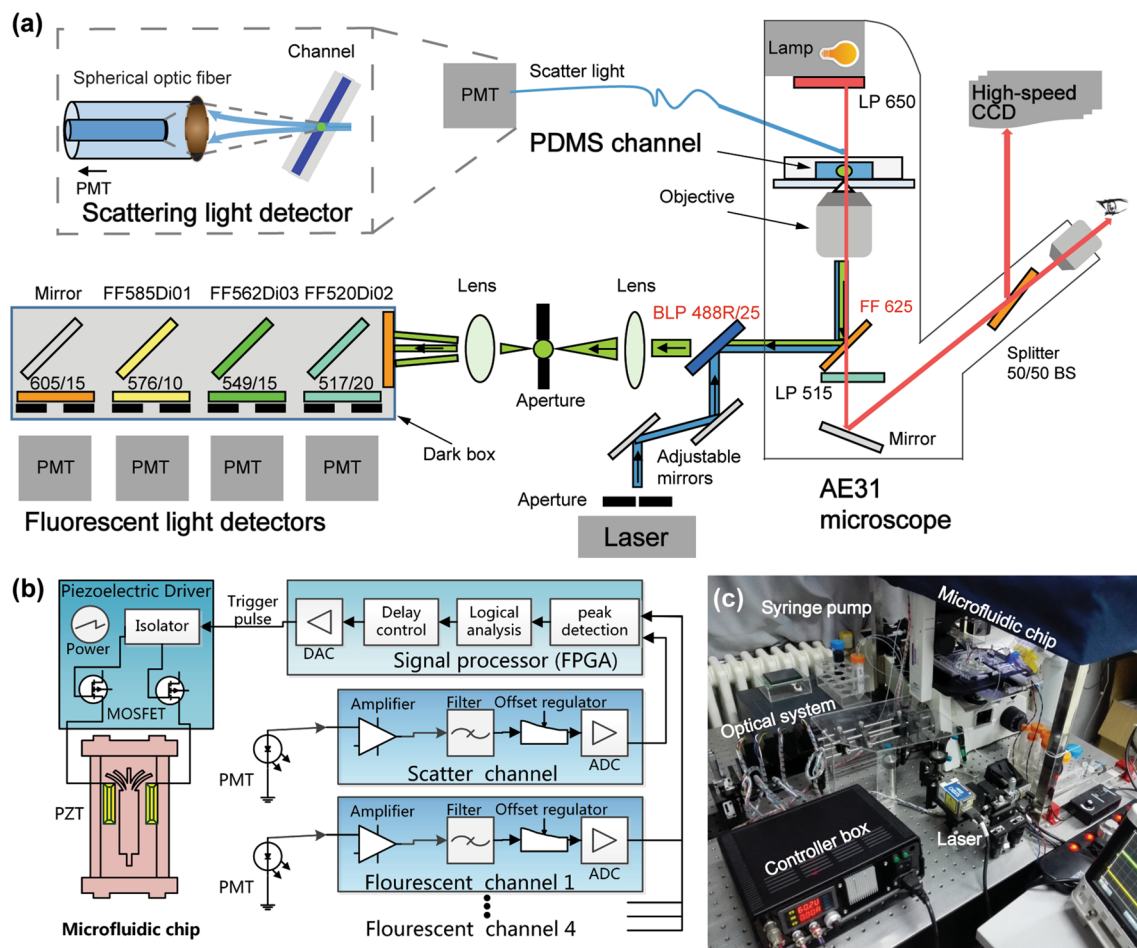


Fig. 2 Layout of the optical and control system. **a** Schematic of the forward scattering and confocal fluorescence detection system. **b** Electronic control system for signal processing and triggering signal generation. **c** Photograph of the μ FACS system

2.2 Optical and control system

The fluorescence-activated cell sorter is comprised of a four-color confocal fluorescence detection system with a forward scattering channel and a sorting actuation control system. The optical system was setup by modifying an inverted microscope (AE31, Motic, Xiamen, China) as illustrated in Fig. 2. Briefly, a 70-mW collimated laser beam (OBIS 488 nm, Coherent, Santa Clara, CA) is first reflected by two adjustable mirrors, and then guided into a $10\times$ objective (NA = 0.3, Leica, Wetzlar, Germany) in the microscope by two dichroic mirrors (BLP 488R/25 nm and FF 625 nm, Chroma, Bellows Falls, VT). The laser beam is focused into a $4\text{-}\mu\text{m}$ -diameter spot on the sorting channel for single-cell illumination. Excited fluorescence is collected by the objective and reflected by the dichroic mirrors into a four-color confocal system, where the light is spatially filtered by a 0.5-mm aperture with two Fourier lenses, and then sequentially directed into four PMTs (photomultiplier tubes) (H9307, Hamamatsu, Shizuoka,

Japan). Four sets of dichroic mirrors and filters are installed in front of four PMTs for narrowing the wavelength ranges to 517 ± 20 nm, 549 ± 15 nm, 576 ± 10 nm, and 605 ± 15 nm accordingly (Chroma). The forward scattering light of the laser beam is collected by an optical fiber with a ball end (FDP100, Polymicro Technologies, Phoenix, AZ) and detected by a PMT (H9307-2, Hamamatsu). The position of the ball end of the fiber can be fine-tuned in three directions so that it is positioned right above the microdevice and aligned to the laser beam with a $200\text{-}\mu\text{m}$ lateral offset. In addition, a high-speed camera (Cube3, Mikrotron, Unterschleissheim, Germany) is installed in front of the microscope for visual verification of the cell sorting process. In the current study, only the forward scattering and the 517-nm fluorescent channel were employed for cell detection.

The schematic of the control system for real-time signal processing and PZT actuating is illustrated in Fig. 2b. The scattering and the fluorescent lights are first transferred into electronic pluses by PMTs with an 80-dB adjustable

pre-amplification, and then magnified in a 20-dB gain after subtraction of background signals. Following the filtration with a 10-kHz Butterworth filter and the adjustment with an offset for matching the input range, these analog signals are converted into digital signals by an 8-bit analog-to-digital converter (ADC) (ADS830, TI, Dallas, TX) at a sampling frequency of 1 MHz, and imported into a FPGA (Spartan-2, Xilinx, San Jose, CA) for a real-time logic analysis. If the signals are detected above the adjustable thresholds, two trigger pulses with an adjustable width of 10–500 μ s are sent to a piezoelectric driving module (shown in Fig. 2b) to actuate two on-chip PZTs, respectively. The width and the amplitude of the driving pulses were carefully optimized to reach a sufficient bending of the PZTs, while minimizing the time consumption in each sorting action.

2.3 Sample preparation

In the initial tests, 10- μ m polymeric microspheres (Duke 4210, Thermo Fisher, Waltham, MA) and 15- μ m fluorescent polymeric microspheres (BM130530, Bangs Laboratory, Fishers, IN) with 480 nm/520 nm excitation/emission wavelengths were employed to calibrate the system performance. In cell sorting experiments, two types of HeLa cells, non-fluorescent and GFP-expressing, were cultured in DMEM medium supplemented with 10% fetal bovine serum (FBS) and 1% penicillin–streptomycin (all from Hyclone, GE, Fairfield, CT) in a cell incubator (MCO-15AC, Sanyo, Japan) at 37 °C with 5% CO₂. Cells were passaged every 2 or 3 days for fewer than 10 passages before abandonment. Prior to use, cells were digested by 0.25% 1 \times Trypsin (Hyclone), washed with phosphate-buffered saline (PBS) (Hyclone), and re-suspended in a mixture of PBS and OptiPrep density gradient medium (D1556, Sigma-Aldrich, St. Louis, MO) in an 84:16 volume ratio. The cell number was counted using a hemocytometer (Hdmed, Yancheng, China) and then diluted to a desired concentration. Prior to cell loading to the device, the samples were gently pipetted and filtered through a 40- μ m cell strainer (Falcon, BD Bioscience, East Rutherford, NJ) to exclude cell clusters.

2.4 Operation procedure and sorting principle

The prepared μ FACS microchip was first assembled in a PMMA manifold and fastened onto the stage of the microscope. The optical fiber was then put back in place above the microchip for scattering light detection. After that, the inlets and the outlets were connected to a dual-channel syringe pump (PHD 2000, Harvard Apparatus, Holliston, MA) and the collection tubes, respectively. Cell or bead samples were loaded into the syringe pump that was connected to the sample input channel, while fresh PBS was

loaded into the syringe to the sheath flow inlet. By fixing the flow rate in the sample channel and adjusting the flows in the sheath flow channels, cells were focused tightly into a single file line along the central line of the sorting channel for detection and sorting.

Since the sorting channel is asymmetrically bifurcated into a wide waste channel and a narrow collection channel (Fig. 1a), unsorted cells flowing along the central line of the sorting channel are going straightly into the waste channel. When a target cell passes the detection point, two pulsed voltage signals with an interval will be sequentially sent to both PZTs after a fixed time delay. This delay corresponds to the time for cell to travel from the detection point to the first sorting nozzle. As illustrated in Fig. 1c, a $-20 V_{p-p}$ actuating signal was first sent to the right PZT, causing the upward bending of the actuator to generate a pulling force. This force can drag the target cell traveling transversely toward the collection channel. After a fixed interval of 0.25 ms, a $+20 V_{p-p}$ signal was sent to the left PZT, leading to the downward bending of the PZT to generate a pushing force. This action can further push the cell transversely to the collection channel. This novel relay sorting using two PZTs can significantly improve the deflection strength while reducing the switching time for each sorting event.

2.5 Result verification and calculation of sorting purity and efficiency

Cell samples were inspected using both a fluorescence microscope (IX71, Olympus, Tokyo, Japan) and a commercial flow cytometry (FCM, FACSCalibur™, BD Biosciences) before and after the sorting experiments. To determine a proper GFP (FITC channel) gating for calculation of purities in the FCM results, the positive (GFP-expressing HeLa cells) and the negative (non-fluorescent HeLa cells) control samples were analyzed separately prior to the mixtures. Using the same set of gating, fluorescent histograms of both the presorting and the post-sorting mixtures were analyzed to calculate the corresponding purities of the GFP cells. And the enrichment factor E was determined using Eq. (1) (Cho et al. 2010):

$$E = \frac{A_s/B_s}{A/B} \quad (1)$$

where A_s/B_s is the purity ratio of the fluorescent to the non-fluorescent cells in the post-sorting mixture, and A/B is the same purity ratio in the presorting mixture. The sorting efficiency P , which represents the positive sorting rate or the sorting accuracy, is defined as the percentage of successfully sorted target cells in the total number of target cells (Chen et al. 2014). If we obtain the purities of target cells in the presorting, the post-sorting, and the waste mixtures

as A , A_s , and A_w from the FCM results, the sorting efficiency can be calculated using Eq. (2) shown below. The detailed calculation process can be found in the supplementary information.

$$P = \frac{A_s(A - A_w)}{A(A_s - A_w)} \quad (2)$$

3 Results and discussion

3.1 Flow focusing and optical analysis

We first characterized the hydrodynamic focusing effect on the μ FACS microchip under different sample-to-sheath flow rate ratios by keeping the sample flow constant while varying the sheath flows. As shown in Fig. S1, when we set the sample flow rate to 1 mL/h and the sheath flow rate to 2, 5, 8, 10, 12, or 15 mL/h, the widths of the resulted central stream were measured as 86, 43, 30, 26, 17, or 13 μ m accordingly. Although narrower stream may lead to a lower coefficient of variation (CV) of the detected signals, we finally employed the ratio of 1:10 instead of 1:15 for the rest of the experiments, as too fast velocity of the particles may cause the increase in the sorting error, as well as the over-dilution of the collected samples.

Once the flow rates for both inlets were determined, FAM fluorescent dyes at a serial of diluted concentrations were introduced into the sample channel and focused into a stream along the central line of the sorting channel for testing the limit of detection of the fluorescent detection system. We let the laser beam sweep across the fluorescence stream by moving the microscope stage and recorded the detected signals. As shown in Fig. S2, even 0.5 nmol/L of FAM can still produce a signal of 1.2 V with a signal-to-noise ratio higher than 3. Next, we injected 15- μ m fluorescent microspheres diluted in PBS with a concentration of 5×10^6 beads/mL to test the fluorescent and the scattering light detectors in our system. The detection spot was positioned at the central line of the sorting channel with a 250- μ m distance downstream the converging junction of the sample and the sheath flow channels. The raw data of the scattering and the fluorescent signals as well as the histograms and the scatter plot are illustrated in Fig. S3, showing a good match between the scattering and the fluorescent peaks. The CV values of the scattering and the fluorescent signals were calculated to be 19.8 and 5.6%, respectively. In comparison with the CVs obtained from the commercial FCM system (<2%), the signal variations in our detection system were worse, due probably to the lack of hydrodynamic focusing of beads in the vertical direction and the low numerical aperture (NA) provided by the optical fiber for the scattering detection.

To further verify the feasibility of performing cell analysis on the chip, we prepared a mixture of non-fluorescent

and GFP-expressing HeLa cells with an initial ratio of 1:1.2 and a concentration of 4×10^6 cells/mL for testing. The sample and the sheath flow rates were set to 1 and 10 mL/h, respectively, resulting in a cell throughput of \sim 1100 cells/s. A portion of the raw data of the flow cytometry results obtained from our detection system is shown in Fig. 3a. As indicated in the dashed boxes, some cells only produced scattering peaks (top trace) without corresponding fluorescence peaks (bottom traces), showing these cells were not expressing GFP. The other scattering peaks have corresponding fluorescence peaks, indicating these cells are fluorescent. The histogram of the fluorescent signals collected in 8 s also clearly displayed two distinct peaks corresponding to two subpopulations (Fig. 3b). The total cell numbers of non-fluorescent and GFP-expressing HeLa cells were 3902 cells and 4636 cells, respectively, which are in concordance with the initial cell ratio of 1:1.2. It should be noticed that the scattering peaks were occasionally dropped out (<1.2%) while the fluorescence still showed up. We believe this is due to the relatively lower numerical aperture of the optical fiber and the one-dimensional focusing of the cells. Nevertheless, these results clearly proved that our optical system is capable of detecting the scattering and the fluorescent lights simultaneously.

3.2 Optimization of chip structures and actuation parameters for cell sorting

To push the sorting rate up to the limit, we need to reduce the deformation of the PZTs during actuation, so that the elapsed time of each sorting action could be shortened. Here we conducted a comprehensive optimization on the microchip structures and the actuation parameters to reach this goal. First, to determine the geometries of the microchips and the types of the PZT actuators, we kept all the available PZTs working at a fixed frequency of 95.4 Hz with a pulse width of 0.5 ms and an actuation amplitude of $40 V_{p-p}$, and then measured the lateral displacement of the central stream with a high-speed CCD camera to evaluate the deflection performance of all the parameters. The rationale behind this optimization method is that by selecting the parameters that can provide the maximal deflection, we can later lower the actuation parameters (the pulse width and the amplitude) in the following experiments to shorten the actuation time as much as possible. As listed in Table 1, the parameters of the PZT, the glass cover, and the PDMS layer were all tested, and the best parameters marked with italic in the table was picked based on their deflection performances.

Next, we noticed that the focused central stream vibrates around the bifurcating junction of the collection and the waste channels back and forth several times after each actuation of the PZTs due to the resetting of the PZT actuators

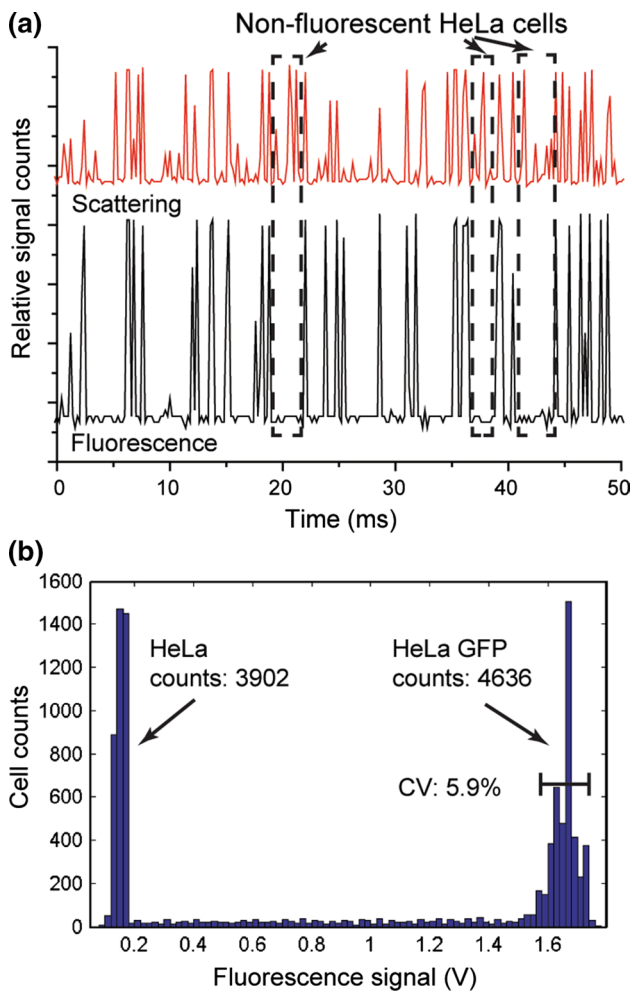


Fig. 3 Flow cytometry analysis of GFP-expressing and non-fluorescent HeLa cell mixtures on the μ FACS chip. **a** A segment of raw data obtained from the μ FACS detection system. Non-fluorescent HeLa cells, as indicated in the *dashed rectangles*, produce only scattering peaks (*top trace*) without corresponding fluorescent peaks (*bottom trace*), while GFP-expressing HeLa cells have aligned peaks in both channels. **b** GFP fluorescence histogram of the cell mixture showing two distinct fluorescent and non-fluorescent cell populations. The detected event counts have the same ratio (4636:3902 \approx 1.19:1) as the initial (1.2:1)

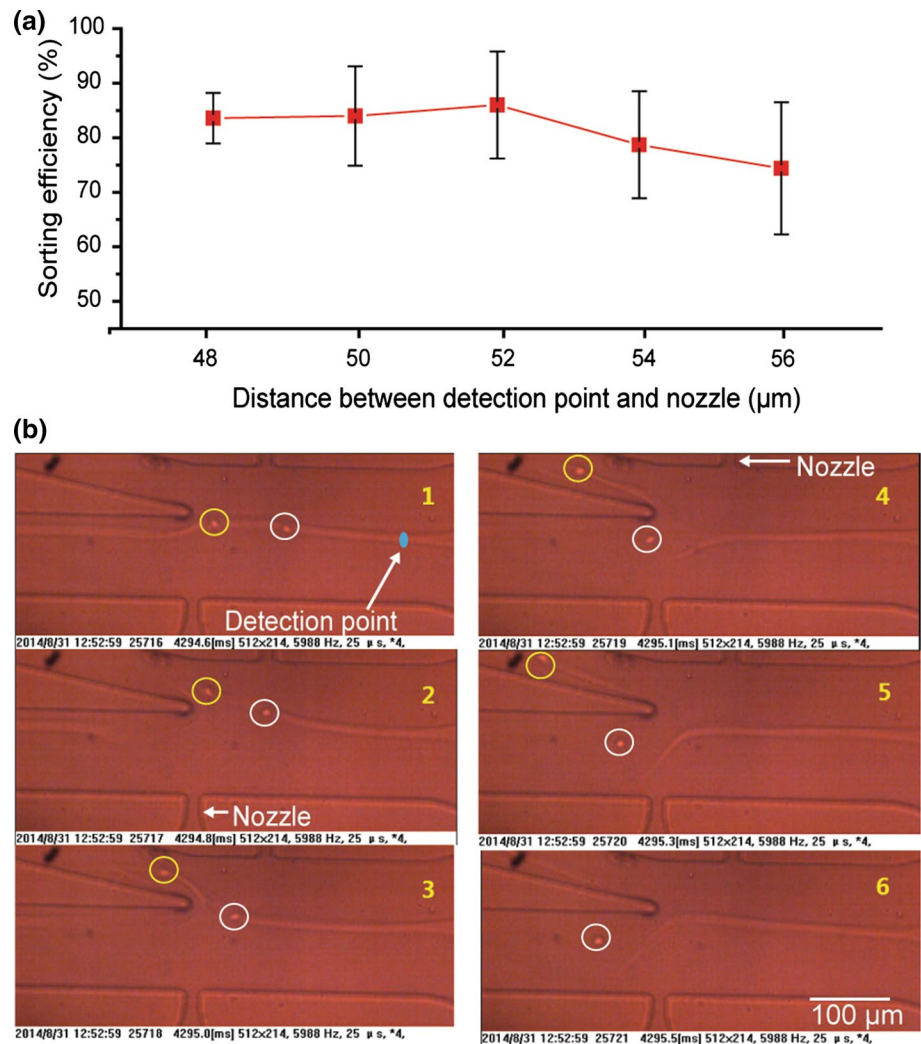
Table 1 Optimization of the μ FACS microchip

Component	Parameter	Deflection distance
PZT	Diameter (mm)	27 > 20 > 15
	Resonant frequency (kHz)	2.6 > 4.0 > 6.5
	Thickness (mm)	0.1 > 0.15 > 0.2
Glass cover	Diameter of actuation holes (mm)	25 > 18 > 12
PDMS layer	Thickness (mm)	4 > 2
	Width of driving nozzle (μ m)	30 > 20

and the inertia of the central stream, resulting in a severely reduced sorting rate. As shown in Video S1, when we just used one side of the PZT to sort cells, the central stream lashes several times around the junction even after the triggering signal to the PZT has been completely removed. One way to alleviate this vibration problem is to further reduce the deformation of the PZT by employing two actuators that work together in a pull–push relay mode, i.e., the right PZT firstly bends upwards to generate a pulling force to the central stream, followed by the downward bending of the left PZT to push the stream further. Video S2 demonstrates that two PZTs working in a synchronization can significantly reduce the back slash of the central stream to a much lower degree, so that the subsequent cells would not mistakenly sorted by the stream vibration. This switching manner can significantly increase the sorting rate. Meanwhile, we carefully optimized the operation parameters for the PZTs (the pulse width, the pulse amplitude, and the pulse interval) to make the lateral displacement of the central stream just enough for an effective sorting with a minimal over-switching. Both PZTs were finally set to work at an actuation pulse width of 0.1 ms, an actuation amplitude of $20 V_{p-p}$, and a pulse interval of 0.25 ms, generating a lateral deflection of $\sim 50 \mu\text{m}$ with a switching time less than 0.8 ms. At this condition, when the cell moving speed is 0.5 m/s, the cells can move about $50 \mu\text{m}$ within the 0.1-ms pulse width along the channel. Since the moving distance is longer than the width of the driving nozzle, the resetting of the PZTs cannot affect the sorted cells. In addition, the back lash of the stream was reduced due to the reduced deformation of the PZTs in each actuation.

Finally, the distance between the detection point and the first actuation nozzle as well as the actuation delay for sending the trigger signals to the PZTs was optimized. Since it is difficult to change the delay that was preset into the control program, we adopted an optimization method that the actuation delay of 0.12 ms was first estimated based on the flow rates and written into the program, then the distance was fine-tuned with a step of $2 \mu\text{m}$ in the range of 48–56 μm . To test the sorting performance, we prepared a mixture of non-fluorescent and GFP-expressing HeLa cells with a ratio of 1:1. As illustrated in Fig. 4a, a 52- μm distance provided the best sorting efficiency for the sorting of the GFP cells, and the result was further verified by visual inspection with the high-speed CCD camera. Representative frames of a switching event are demonstrated in Fig. 4b and Video S3, showing two consecutive cells with a space interval of 120 μm were successfully separated. The first GFP-expressing cell was accurately pushed into the collection channel, while the second non-fluorescence

Fig. 4 Optimization and verification of on-chip cell sorting using two piezoelectric actuators. **a** Optimization of distance between the detection point and the first actuation nozzle. In the range of 48–56 μm , the distance of 52 μm provided the best sorting efficiency. **b** Representative video frames of on-chip cell sorting using the PZTs. The detection point was indicated with a *blue dot*. The first GFP-expressing cell was accurately pushed into the collection channel, while the second non-fluorescence one was still in the waste channel. The distance between these two cells was about 120 μm . The video was recorded in 5988 Hz (color figure online)



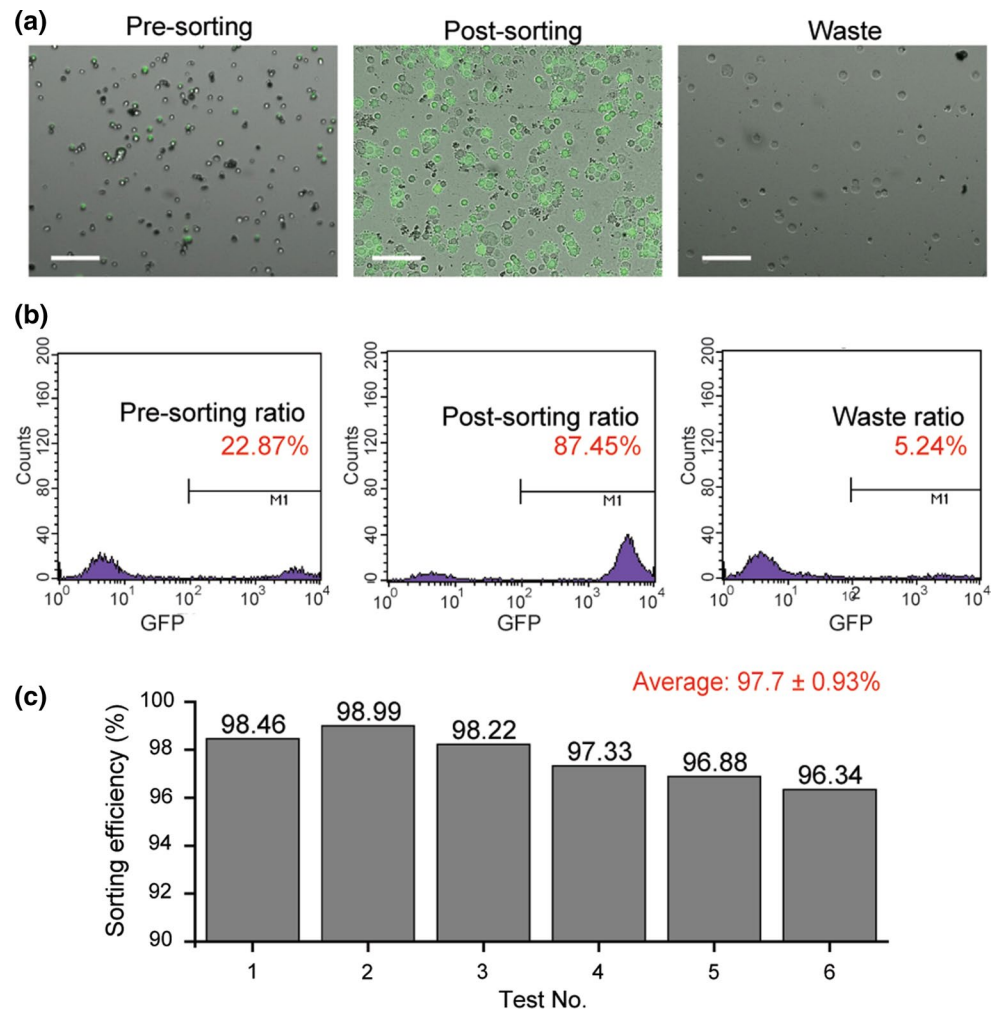
one was still in the waste channel. The actual response time of a single actuation was calculated to be 0.8 ms based on the frame rate, leading to a sorting rate up to 1250 cells/s. In addition, we examined a series of frames in 0.3 s one by one and found that 56 cells were successfully separated within 115 cells, which testified a purity of over 95% (only 30% of the events were recorded with the camera setting of 5988 frames/s at an exposure of 50 μs).

3.3 Enrichment of GFP-expressing HeLa cells

Following the optimization of our μFACS cell sorter, we conducted an automated cell sorting of GFP-expressing HeLa cells from non-fluorescent cell background at a total cell concentration of 6×10^6 cells/mL to more critically test the system. In this experiment, we increased the sample flow rate to 1.5 mL/h with a corresponding sheath flow rate of 15 mL/h, resulting in a detection throughput of 2500 cells/s and an estimated cell velocity of ~ 0.5 m/s. Other operation parameters were finely optimized to

ensure the successful cell sorting under a high-flow condition. Although the sorting rate of the PZT actuators is still around 1250 cells/s, the sorting efficiency should be similar to the previous test as the fluorescent target cells only account for less than 50% of the mixture. Once the experiments were finished, the purities of the GFP cells in the presorting and the post-sorting cell mixture were first quantified using a fluorescent microscope and then validated by the commercial BD FACS system. As shown in Fig. 5a, the relative cell numbers in the captured microscope images were manually counted, indicating the purities of the fluorescent cells are 24% in the presorting mixture, 89% in the sample collected from the collection channel (the post-sorting mixture), and $<1\%$ in the sample from the waste channel (the waste mixture). The results obtained from the BD flow cytometer confirmed that the purities of the GFP cells were 22.87% in the presorting mixture, 87.45% in the collection channel (the post-sorting mixture), and 5.24% in the waste channel (the waste mixture) (Fig. 5b). Since not every single target cells can be correctly sorted, our system

Fig. 5 Fluorescence-based cell sorting of GFP-expressing HeLa cells performed on the μ FACS system. **a** Combined bright-field and fluorescent micrographs of the presorting, the post-sorting, and the waste mixtures (*scale bars* 100 μ m). **b** Scatter plots of the presorting, the post-sorting, and the waste mixtures. All the results were analyzed using the same gate settings. **c** Six identical cell mixtures consecutively sorted on the μ FACS system, showing a stable sorting efficiency of $97.7 \pm 0.93\%$



was best used for cell enrichment instead of extremely rare cell separation. To further demonstrate the stability of our μ FACS system in cell sorting, we consecutively analyzed six identical samples with a running time of 20 min for each test. The results in Fig. 5c demonstrated that the run-to-run sorting efficiency provided by the μ FACS microchip stayed roughly stable in $97.7 \pm 0.93\%$ under the same flow and operation conditions.

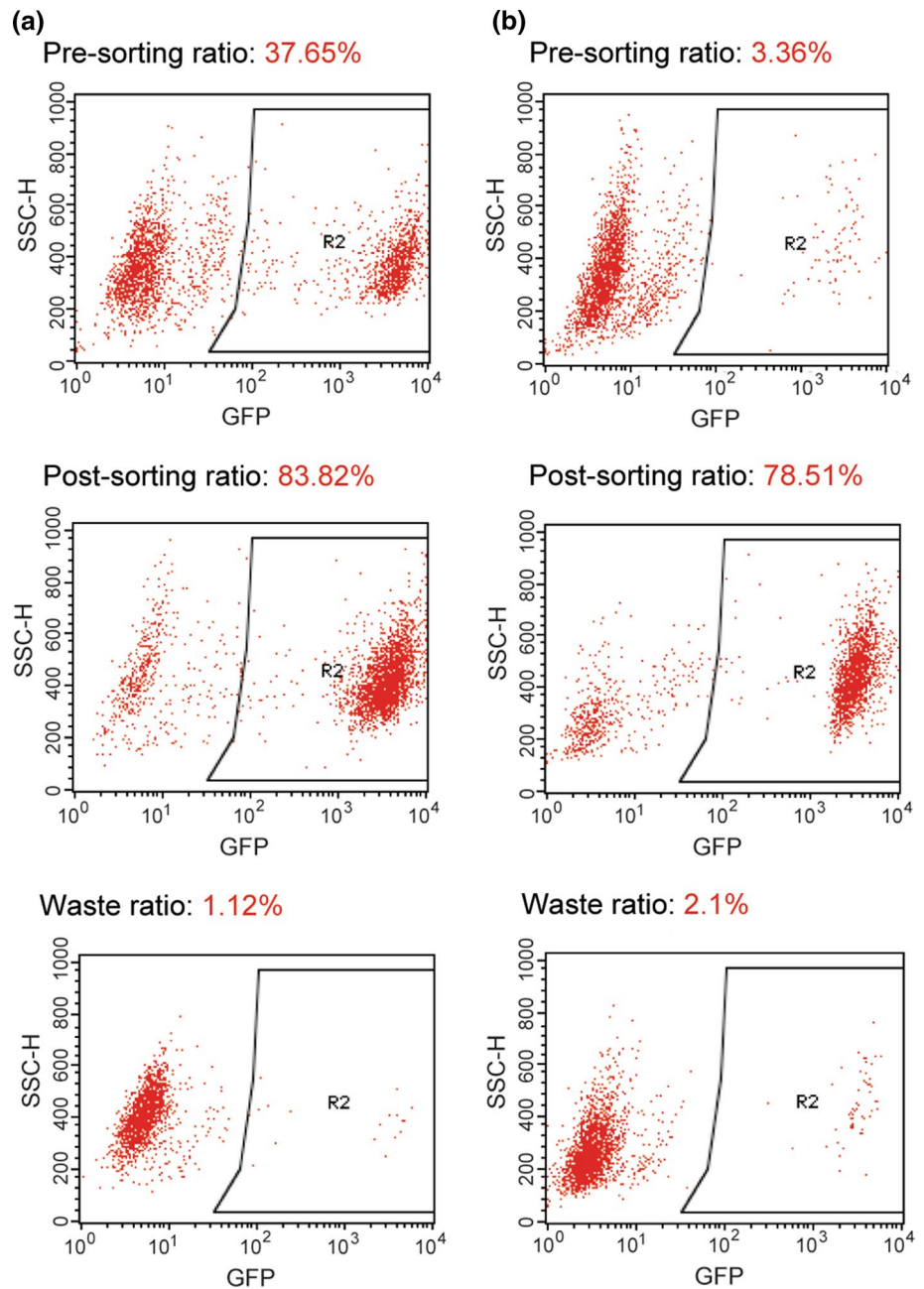
Next, to verify the capability of the μ FACS microchip for analyzing samples with various cell purities, we prepared two cell mixtures containing 37.65 and 3.36% GFP HeLa cells, representing the cases where target cells are in a high or low purity, respectively. As shown in Fig. 6, the GFP-expressing cells in both samples can be effectively enriched up to 83.82 and 78.51%, respectively. Especially for the low-purity sample (3.36%), an enrichment factor of 105 could be obtained on our μ FACS system. In the current study, total of three cell mixtures containing 3.36, 22.87, and 37.65% target cells were sorted on our system. The average post-sorting ratio was $83.3 \pm 4.5\%$, which is more stable than those demonstrated in previous studies.

However, more optimizations are needed in order to further improve the performance of the system. This work successfully established the feasibility of performing fluorescence-based cell enrichments on a microfabricated device with integrated PZT actuators.

4 Conclusion

We have successfully developed a piezo-actuation-based μ FACS system coupled with a forward scattering and confocal fluorescence detection system for high-performance single-cell detection and sorting. By employing a novel two-PZT relay switching structure, our cost-effective cell sorter has demonstrated a high detection throughput (>2500 cells/s), a high sorting rate (1250 cells/s), and a high sorting efficiency ($\sim 98\%$) for fluorescence-based mammalian cell analysis and enrichment. Although the device demonstrated here is a laboratory prototype, it has already provided several extraordinary advantages compared with the conventional FACS. First, the integrated, low-cost microchip can

Fig. 6 Flow cytometry analyses of the presorting, the post-sorting, and the waste cell mixtures obtained from the μ FACS system. Two cell mixtures containing **a** 37.65% and **b** 3.36% GFP HeLa cells were analyzed, and the collected samples from the microchip were quantitated using the BD FACS instrument. The results demonstrate that both samples can be effectively enriched up to the purities of **a** 83.82% and **b** 78.51%, respectively. For the low-purity sample, an enrichment factor of 105 was successfully obtained



be used as a disposable device for preventing the run-to-run contamination. As summarized in Table S1, the material cost for each microdevice is around \$ 5.66, in which the integrated PZT actuators cost about one-third of the price (\$1.88). While the device cost can be further reduced by employing external PZT actuators, this fully integrated design can provide much higher reproducibility regarding the sorting performance. Nevertheless, the cost with the disposable PZTs is already much lower than flow cuvettes used in the commercial FACS systems. Second, the completely enclosed microstructures for cell sorting can effectively eliminate the hazardous aerosol contamination.

Third, the dramatic size reduction in the flow and sorting part in our microfabricated system together with the compact detection system developed previously by our group (Zhuang et al. 2016) will make this technology attractive to many resource-limited applications, such as point-of-care diagnosis. In the future, we believe the performance of our system can be significantly improved by employing the four-color fluorescent detection, by designing a more sophisticated forward and side scattering system, and by incorporating 3D focusing structures that have demonstrated elsewhere (Amini et al. 2014; Mao et al. 2009). More characterizations, such as sorting different cell types

and the cell damage evaluation, need to be done. In addition, the microfabricated device also possesses the potential of integrating with sample preprocessing structures for the analysis of more challenging samples, such as circulating tumor cells.

Acknowledgements We thank Dong Wang and Lei Wang at the National Engineering Research Center for Beijing Biochip Technology for their valuable advices on system development. We also thank the Cell Facility in the Tsinghua Center of Biomedical Analysis for the assistance on the BD FACSCalibur™ instrument. Microchip fabrication was conducted at the Microfabrication Laboratory, the National Engineering Research Center for Beijing Biochip Technology, China. This work was supported by the National Natural Science Foundation of China (No. 81341081).

References

- Amini H, Lee W, Di Carlo D (2014) Inertial microfluidic physics. *Lab Chip* 14:2739–2761
- Cao Z et al (2013) Droplet sorting based on the number of encapsulated particles using a solenoid valve. *Lab Chip* 13:171–178
- Chen CH, Cho SH, Chiang HI, Tsai F, Zhang K, Lo YH (2011) Specific sorting of single bacterial cells with microfabricated fluorescence-activated cell sorting and tyramide signal amplification fluorescence in situ hybridization. *Anal Chem* 83:7269–7275
- Chen Y, Wu TH, Kung YC, Teitell MA, Chiou PY (2013) 3D pulsed laser-triggered high-speed microfluidic fluorescence-activated cell sorter. *Analyst* 138:7308–7315
- Chen Y, Chung AJ, Wu TH, Teitell MA, Di Carlo D, Chiou PY (2014) Pulsed laser activated cell sorting with three dimensional sheathless inertial focusing. *Small* 10:1746–1751
- Cho SH, Chen CH, Tsai FS, Godin JM, Lo YH (2010) Human mammalian cell sorting using a highly integrated micro-fabricated fluorescence-activated cell sorter (microFACS). *Lab Chip* 10:1567–1573
- Duffy DC, McDonald JC, Schueller OJ, Whitesides GM (1998) Rapid prototyping of microfluidic systems in poly(dimethylsiloxane). *Anal Chem* 70:4974–4984
- Franke T, Braunmuller S, Schmid L, Wixforth A, Weitz DA (2010) Surface acoustic wave actuated cell sorting (SAWACS). *Lab Chip* 10:789–794
- Fu AY, Spence C, Scherer A, Arnold FH, Quake SR (1999) A microfabricated fluorescence-activated cell sorter. *Nat Biotechnol* 17:1109–1111
- Fu AY, Chou HP, Spence C, Arnold FH, Quake SR (2002) An integrated microfabricated cell sorter. *Anal Chem* 74:2451–2457
- Gawad C, Koh W, Quake SR (2016) Single-cell genome sequencing: current state of the science. *Nat Rev Genet* 17:175–188
- Godin J, Chen C-H, Cho SH, Qiao W, Tsai F, Lo Y-H (2008) Microfluidics and photonics for bio-system-on-a-chip: a review of advancements in technology towards a microfluidic flow cytometry chip. *J Biophotonics* 1:355–376
- Gray DW, Gohde W, Carter N, Heiden T, Morris PJ (1989) Separation of pancreatic islets by fluorescence-activated sorting. *Diabetes* 38(Suppl 1):133–135
- Ho CT, Lin RZ, Chang HY, Liu CH (2005) Micromachined electrochemical T-switches for cell sorting applications. *Lab Chip* 5:1248–1258
- Holmes KL et al (2014) International society for the advancement of cytometry cell sorter biosafety standards. *Cytom A* 85:434–453
- Ibrahim SF, van den Engh G (2003) High-speed cell sorting: fundamentals and recent advances. *Curr Opin Biotechnol* 14:5–12
- Jaye DL, Bray RA, Gebel HM, Harris WA, Waller EK (2012) Translational applications of flow cytometry in clinical practice. *J Immunol* 188:4715–4719
- Kim HJ, Moon HS, Kwak BS, Jung HI (2011) Microfluidic device to separate micro-beads with various fluorescence intensities. *Sens Actuators B Chem* 160:1536–1543
- MacDonald MP, Spalding GC, Dholakia K (2003) Microfluidic sorting in an optical lattice. *Nature* 426:421–424
- Macey MG (ed) (2007) *Flow cytometry: principles and applications*. Humana Press Inc., Totowa
- Magbanua MJ, Park JW (2013) Isolation of circulating tumor cells by immunomagnetic enrichment and fluorescence-activated cell sorting (IE/FACS) for molecular profiling. *Methods* 64:114–118
- Mao X, Lin SC, Dong C, Huang TJ (2009) Single-layer planar on-chip flow cytometer using microfluidic drifting based three-dimensional (3D) hydrodynamic focusing. *Lab Chip* 9:1583–1589
- Naujok O, Kaldrack J, Taivankhuu T, Jorns A, Lenzen S (2010) Selective removal of undifferentiated embryonic stem cells from differentiation cultures through HSV1 thymidine kinase and ganciclovir treatment. *Stem Cell Rev* 6:450–461
- Osborne GW (2011) Recent advances in flow cytometric cell sorting. *Methods Cell Biol* 102:533–556
- Perroud TD, Kaiser JN, Sy JC, Lane TW, Branda CS, Singh AK, Patel KD (2008) Microfluidic-based cell sorting of *Francisella tularensis* infected macrophages using optical forces. *Anal Chem* 80:6365–6372
- Pfeffer F, Dombkowski D (2009) Advances in complex multiparameter flow cytometry technology: applications in stem cell research. *Cytom B Clin Cytom* 76:295–314
- Schmid I, Lambert C, Ambrozak D, Peretto SP (2007) Standard safety practices for sorting of unfixed cells. *Curr Protoc Cytom* 3.6.1–3.6.20. doi:10.1002/0471142956.cy0306s39
- Sciambi A, Abate AR (2015) Accurate microfluidic sorting of droplets at 30 kHz. *Lab Chip* 15:47–51
- Shapiro HM (ed) (2005) *Practical flow cytometry*, 4th edn. Wiley Online Library, New York
- Shirasaki Y, Tanaka J, Makazu H, Tashiro K, Shoji S, Tsukita S, Funatsu T (2006) On-chip cell sorting system using laser-induced heating of a thermoreversible gelation polymer to control flow. *Anal Chem* 78:695–701
- Sugino H, Ozaki K, Shirasaki Y, Arakawa T, Shoji S, Funatsu T (2009) On-chip microfluidic sorting with fluorescence spectrum detection and multiway separation. *Lab Chip* 9:1254–1260
- Wang MM et al (2005) Microfluidic sorting of mammalian cells by optical force switching. *Nat Biotechnol* 23:83–87
- Wolff A et al (2003) Integrating advanced functionality in a microfabricated high-throughput fluorescent-activated cell sorter. *Lab Chip* 3:22–27
- Wu L, Chen P, Dong Y, Feng X, Liu BF (2013) Encapsulation of single cells on a microfluidic device integrating droplet generation with fluorescence-activated droplet sorting. *Biomed Microdevices* 15:553–560
- Wyatt Shields C IV, Reyes CD, Lopez GP (2015) Microfluidic cell sorting: a review of the advances in the separation of cells from debulking to rare cell isolation. *Lab Chip* 15:1230–1249
- Yu ZT, Aw Yong KM, Fu J (2014) Microfluidic blood cell sorting: now and beyond. *Small* 10:1687–1703
- Zhuang B et al (2016) A fully integrated and automated microsystem for rapid pharmacogenetic typing of multiple warfarin-related single-nucleotide polymorphisms. *Lab Chip* 16:86–95